Influence of septal penetration and scatter on ^{123}I SPECT collimator-detector response modeling

J.B. Moody[1] , Y.K. Dewaraja[2], J.A. Fessler[2], E.P. Ficaro[1,2]

[1] INVIA Medical Imaging Solutions, Ann Arbor, MI, [2]University of Michigan Health System, Ann Arbor, MI

INVIA Medical Imaging Solutions

University of Michigan Health System

OBJECTIVE

To study the relative contributions of corrections for septal penetration and scatter on 3D-OS-EM reconstruction of cardiac ^{123}I-meta-iodobenzylguanidine (MIBG) SPECT images with collimator-detector response modeling.

INTRODUCTION

- Septal penetration and scatter of high energy photons are well-known problems for LEHR-collimated ^{123}I SPECT [1,2].
- Combined with high extra-cardiac uptake of ^{123}I-MIBG , this results in poor cardiac contrast and poor image quality for FBP images.
- To improve quantitative accuracy and image quality, these physical effects can be compensated by modeling the collimator-detector response in an iterative reconstruction algorithm.
- In this study we developed empirical models of collimator-detector response (CDR) to evaluate the influence of compensating septal penetration and scatter on image resolution and contrast.

METHODS

CDR Models

- Projections of an ^{123}I point source in air were acquired at various detector distances on a Siemens Symbia SPECT/CT with LEHR collimator [3].
- Each projection was scatter corrected (TEW) and fit to three 2D functions (Fig.1):
  - 2-parameter model: $f(\mathbf{r}) = A\exp[-(\mathbf{r}-\mathbf{r}_0)^2/2B^2]$ **G**
  - 4-parameter model: $f(\mathbf{r}) = A\exp[-(\mathbf{r}-\mathbf{r}_0)^2/2B^2] + C\exp[-(\mathbf{r}-\mathbf{r}_0)/D]$ **SP1**
  - 6-parameter model: $f(\mathbf{r}) = A\exp[-(\mathbf{r}-\mathbf{r}_0)^2/2B^2] + C\exp[-(\mathbf{r}-\mathbf{r}_0)/D] + E\exp[-\exp(-(\mathbf{r}-\mathbf{r}_0)/F)]$ **SP2**
- The models of the projection data were fit to functions of detector distance (Fig.2):
  - Amplitude parameters (A, C, E) were fit to a decaying exponential vs distance.
  - Width parameters (B, D, F) were fit to a linear function vs distance.

Phantoms

- Three ^{123}I phantom datasets were acquired:
  - Point source in scattering medium (20 cm diameter water cylinder).
  - Cardiac torso phantom (Data Spectrum Corp, NC) with heart, lung, and liver inserts:
    - Activity concentration ratio: (Heart:Lung:Liver:BG) = 20:5:10:1 **P1 (normal uptake)**
    - Activity concentration ratio: (Heart:Lung:Liver:BG) = 15:8:10:1 **P2 (abnormal uptake)**
- 20% photopeak (159 keV), 6% side windows for TEW scatter correction.

Image Reconstruction and Evaluation

- Projection data was reconstructed using 3D-OS-EM with attenuation correction (AC), using each of the 3 CDR models, and with/without TEW scatter correction (SC) [4], resulting in 6 image volumes for each data set.
- The point source phantom FWHM and FWTM was evaluated as a function of iteration.
- The torso phantom images were assessed by maximizing the contrast-to-noise ratio between myocardium and ventricle with respect to OS-EM iteration:

$$CNR = (Myo - Ventricle)/Ventricle$$

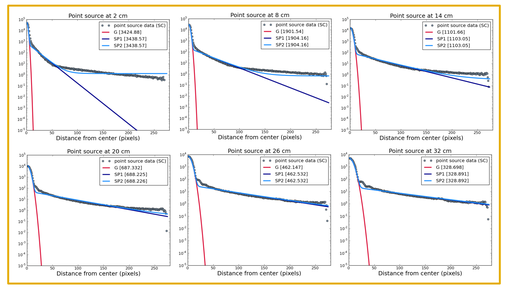

Figure 1: Radial averages of point source projections in air, with fits of three analytic models: G = gaussian; SP1 = (gaussian + exp); SP2 = (gaussian + exp + exp(exp)). Models SP1 and SP2 include geometric and septal penetration effects, while Model G only includes geometric effects.

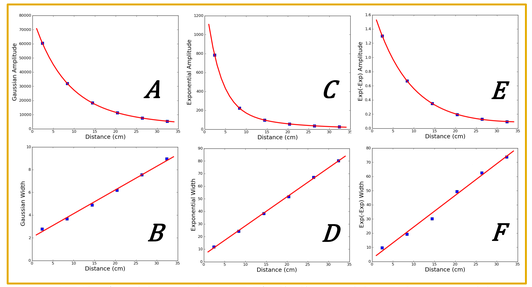

Figure 2: Fits of model parameters, A – F, for the three analytic point source models in Fig.1 as functions of detector distance.

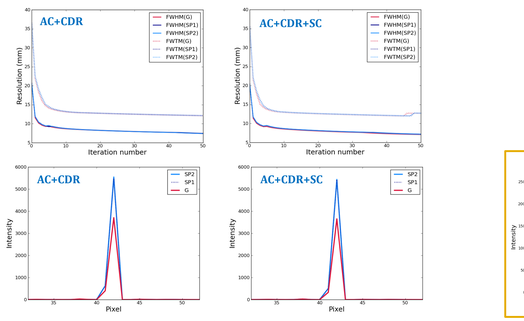

Figure 3: Point Source in Water. Resolution versus OS-EM iteration with and without SC (upper two plots) showed virtually no difference in FWHM or FWTM between models G, SP1 and SP2. Profiles through the point source (lower plots) similarly showed no difference in resolution, although models SP1 and SP2 produced peaks of consistently higher amplitude than model G.

RESULTS

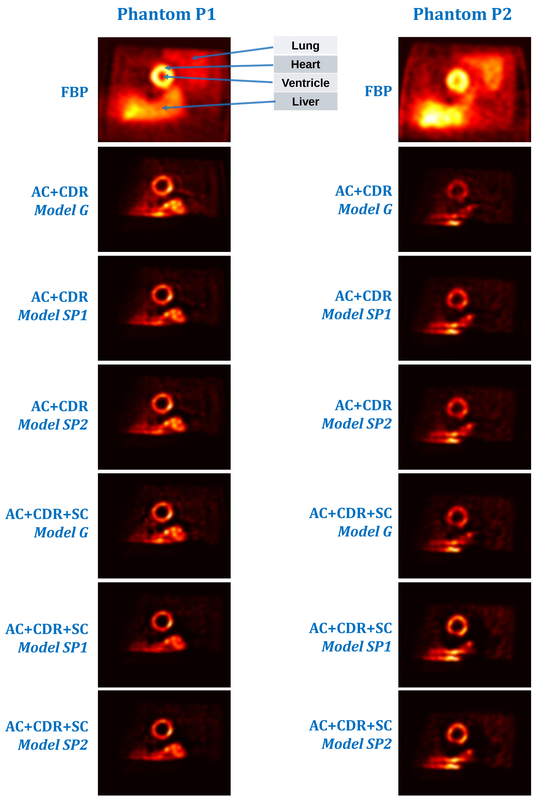

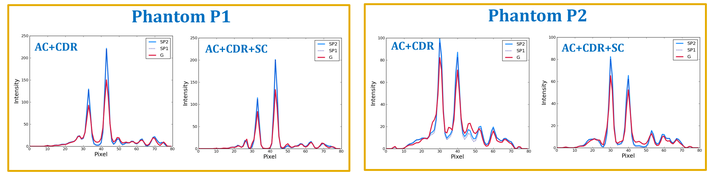

Figure 4: Images and horizontal profiles through the heart center. Short axis images (top) and profiles (bottom) are shown for each phantom and reconstructions with FBP and OS-EM (AC+CDR or AC+CDR+SC) and each CDR model. Contrast between the heart wall and ventricle improved with addition of septal penetration to the CDR model as well as TEW scatter correction in the reconstruction.

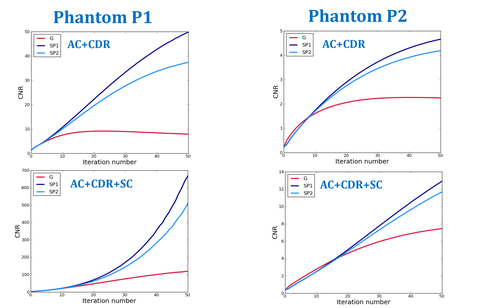

Figure 5: CNR versus OS-EM iteration. The CDR models that included septal penetration (SP1, SP2) produced significantly higher CNR than model G over all iterations and both phantoms..

Phantom	Model G	Model SP1	Model SP2	SC + Model G	SC + Model SP1	SC + Model SP2
P1	9.15	49.80	37.39	119.07	667.14	509.59
P2	2.27	4.66	4.19	7.45	12.91	11.69

Table 1: Maximum CNR. The CDR models that included septal penetration (SP1, SP2) produced maximum cardiac CNR increases of between 4-5x(Phantom P1) and 1.5-2x (Phantom P2) relative to that of model G. The addition of scatter correction (SC) resulted in additional CNR increases of similar relative magnitude.

CONCLUSIONS

- The CDR models that included the effects of septal penetration (SP1 and SP2) provided better overall fits to the point source in air data (Fig.1, 2).
- The point source in scattering media demonstrated no apparent change in resolution between all three CDR models, consistent with the fact that all three incorporated the same geometric response. (Fig.3)
- The CDR model that included only geometric effects (model G) produced a significant improvement in CNR and resolution compared to FBP images (Fig.4)
- Modeling septal penetration in the CDR function with either model SP1 or SP2 resulted in a further improvement in CNR, which depended on the activity distribution (Fig.5)
- The percent CNR increase due to scatter correction alone (SC+model G), was approximately the same as that due to modeling septal penetration in the CDR function (Table 6).
- To obtain maximal CNR benefit with ^{123}I CDR compensation, septal penetration modeling with scatter correction should be used.

REFERENCES

[1] Y. Du, B. M. W. Tsui, and E. C. Frey, "Model-based compensation for quantitative 123I brain SPECT imaging," Physics in Medicine and Biology, vol. 51, no. 5, pp. 1269-1282, Mar. 2006.

[2] R. Van Holen, S. Staelens, and S. Vandenberghe, "SPECT imaging of high energy isotopes and isotopes with high energy contaminants with rotating slat collimators," Medical Physics, vol. 36, no. 9, pp. 4257-4267, 2009.

[3] K. F. Koral, A. Yendiki, and Y. K. Dewaraja, "Recovery of total I-131 activity within focal volumes using SPECT and 3D OSEM," Physics in Medicine and Biology, vol. 52, no. 3, p. 777, 2007.

[4] Y. K. Dewaraja, M. Ljungberg, and J. A. Fessler, "3-D Monte Carlo-based scatter compensation in quantitative I-131 SPECT reconstruction," Nuclear Science, IEEE Transactions on, vol. 53, no. 1 Part 1, pp. 181-188, 2006.